## Complexome profiling identifies changes in mitochondrial supercomplexes in murine heart failure

Fong-McMaster, Claire; McIlroy, Ella; Levesque, Michelle M.; Myers, Stephanie; Pulente, Serena M.; Gahla, Gurrose; Lorenzen-Schmidt, Ilka; Cuperlovic-Culf, Miroslava; Haqqani, Arsalan S.; Mulvihill, Erin E.; Harper, Mary-Ellen



**Publisher's version / Version de l'éditeur:**

https://doi.org/10.1152/ajpheart.00278.2025

*American Journal of Physiology-Heart and Circulatory Physiology, 2025-06-30*

# Complexome profiling identifies changes in mitochondrial supercomplexes in murine heart failure

Claire Fong-McMaster[1,2,3], Ella McIlroy[1,2], Michelle M. Levesque[1,2,3], Stephanie Myers[1,2], Serena M. Pulente[1,3], Gurrose Gahla[1], Ilka Lorenzen-Schmidt[3], Miroslava Cuperlovic-Culf[1,2,4], Arsalan S. Haqqani[5], Erin E. Mulvihill[1,2,3,6,7], and Mary-Ellen Harper[1,2,3]

[1]Department of Biochemistry, Microbiology and Immunology, University of Ottawa, Ottawa, Ontario, Canada

[2]Ottawa Institute of Systems Biology, University of Ottawa, Ottawa, Ontario, Canada

[3]University of Ottawa Heart Institute, Ottawa, Ontario, Canada

[4]Digital Technologies Research Centre, National Research Council Canada, Ottawa, Ontario, Canada

[5]Human Health Therapeutics Research Centre, National Research Council Canada, Ottawa, Ontario, Canada

[6]Montreal Diabetes Research Group, Montreal, Quebec, Canada

[7]Centre for Infection, Immunity and Inflammation, Ottawa, Ontario, Canada

Running title: Mitochondrial supercomplexes in murine heart failure

Correspondence:

Mary-Ellen Harper, PhD

mharper@uottawa.ca, 613-562-5800 ext. 8458

University of Ottawa Faculty of Medicine, 451 Smyth Rd, RGN3510B, Ottawa, Ontario, Canada, K1H 8M5

**Abstract**

Heart failure is characterized by metabolic derangements such as altered substrate metabolism and mitochondrial dysfunction. Mitochondrial supercomplexes, which are higher-order molecular structures comprised of multi-subunit complexes of the electron transport chain, are decreased in heart failure. To investigate the supercomplex proteome composition in heart failure, we used an *in vivo* myocardial infarction (MI) model in which mice exhibited reduced cardiac function, confirmed by two-dimensional echocardiography at 4 weeks post-infarction. To assess proteins within supercomplexes, we used an emerging technique known as complexome profiling. This technique involved separating out mitochondrial protein complexes using Blue-Native PAGE combined with mass spectrometry to identify proteins within supercomplex gel bands. We identified band-dependent decreases or increases in the relative abundance of subunits of the electron transport chain between MI and sham mice. Decreased abundance of proteins involved in α-ketoglutarate dehydrogenase metabolism including DLST was also identified in the supercomplex bands of MI mice compared to sham mice. In addition, decreased abundance of redox-related proteins such as SOD2 and changes in ribosome protein subunits were identified in the MI mitochondria. In conclusion, we identified changes in the mitochondrial supercomplex proteome in a murine model of heart failure, providing insight and novel mechanisms that may be contributing to the metabolic dysfunction in heart failure.

**New and Noteworthy**

This study identified novel changes in the proteome of mitochondrial supercomplexes in a murine model of heart failure including alterations in the relative abundance of metabolic protein

complexes, redox proteins, and ribosomal proteins. These findings provide new insights into potential mechanisms that may contribute to metabolic dysfunction in heart failure.

**Keywords**

Respirasome, Blue-Native PAGE, oxidative phosphorylation, mass spectrometry, cardiomyopathy

## Introduction

Heart failure is a complex and chronic disease with many underlying factors. Central to the pathogenesis of this disease are changes in energy metabolism. The oxidative phosphorylation (OXPHOS) machinery in the inner mitochondrial membrane, which drives ATP production, consists of four electron transport chain oxidoreductase complexes (CI-CIV) and the ATP synthase complex (CV). These oxidoreductase complexes assemble as higher-order structures known as respiratory supercomplexes in multiple stoichiometric arrangements of $CI_1CIII_2CIV_{1-4}$, $CI_1CIII_2$ and $CIII_2CIV_{1-2}$ (1). Since their initial characterization, there has been strong evidence that SCs assemble in metabolically active tissues such as the heart (2–6).

Disassembly of supercomplexes is observed in many cases of cardiac dysfunction including heart failure (7), atrial fibrillation (8), ischemic reperfusion (9–11), and aging (4). In contrast, NDUFAB1, an accessory subunit of CI, contributes to supercomplex assembly, and has been shown to be cardioprotective (5). Myocardial supercomplex assemblies also dynamically mediate metabolic protection in response to ischemia/reperfusion (12). Earlier work investigating mechanisms underlying cardioprotective strategies showed no changes in overall supercomplex abundance but greater levels of cytochrome-c oxidase subunit within supercomplexes in the cardioprotective conditions (13). Other work has suggested that *ex vivo* cardiac function is not impacted by supercomplex assembly (14). Recent work with a point mutant mouse model disrupting supercomplex assembly demonstrated no changes in bioenergetic capacity in cardiac mitochondria (15). Altogether, findings highlight complexities and controversies in resolving the structural and functional implications of mitochondrial supercomplexes in the heart.

Currently approaches to study mitochondrial supercomplexes involve mild solubilization of mitochondria followed by gel electrophoresis, a technique known as Blue-Native or Clear-Native PAGE (2, 16). This gel-based technique is paired with immunoblotting to detect specific subunits within the electron transport chain or direct incubation with various substrates to measure in-gel activity of the complexes (17). Technical advances in combining Blue-Native PAGE and liquid chromatography with tandem mass spectrometry have revealed the proteome composition of mitochondrial supercomplexes in the murine heart (18, 19), in murine skeletal muscle in response to exercise (20), and in fibroblasts of patients with mitochondrial disorders (21). In addition, recent datasets have been developed to comprehensively identify and predict mitochondrial complexes (22, 23). Our results here serve as the first proteomic resource for mitochondrial supercomplex proteome composition in heart failure. We identify altered abundance of electron transport chain, metabolic, redox, and ribosomal proteins in the failing heart, highlighting novel mechanisms that may contribute to the metabolic landscape of heart failure.

## Methods

### Animal studies

All animal studies were approved by the Animal Care Committee of the University of Ottawa (UOHI-AUP-4381) and conducted with the principles of the Canadian Council of Animal Care. Male and female CD-1 mice (8 weeks) were obtained from Charles River. All mice were housed in a 12-hour/12-hour light/dark cycle with *ad libitum* access to chow (Teklad 2018) and water. Myocardial infarction (MI) surgery was performed as previously described (24).

**Myocardial infarction model**

Myocardial infarction was induced using a surgical model of heart failure involving the permanent ligation of the left anterior descending coronary artery (LAD). Mice were treated pre-operatively with 1.2mg/kg buprenorphine (1.2mg/kg; subcutaneous) and meloxicam (5mg/kg) and treated with meloxicam (5mg/kg) 24hr and 48hr post-surgery. Mice were anesthetized with isoflurane (2%) and intubated by intra-tracheal insertion of a 20G flexible catheter. The mice were maintained on a ventilator set to 130 breaths per minute throughout the procedure.

The mouse was positioned supine on a heating pad on the surgical platform. The chest cavity was opened and maintained open with a chest retractor to expose the heart. The LAD was visualized underneath a surgical microscope and ligated 1-2mm below the tip of the left atrium using a 7-0 silk. Infarction was confirmed by the loss of color on the anterior wall of the left ventricle. The chest retractor was moved, and the muscles and skin were closed with 6-0 absorbable nylon sutures. Sham mice underwent the same procedure without ligation of the LAD. Mice were moved to a 30°C recovery chamber and returned to housing rooms after recovery.

**2-Dimensional echocardiography**

Cardiac functional parameters were measured using a VEVO3100 System (Visual Sonics, Toronto, Canada). Mice were anesthetized with 2-3% isoflurane and 1.5 L/min of oxygen and maintained on a heated (37°C) imaging platform. Ejection fraction, end-systolic volume, end-

diastolic volume, and akinetic area were measured using 2-dimensional parasternal long axis imaging. All data analysis was completed using VevoLAB (5.10.0).

**Mitochondrial isolation**

Mitochondrial from the remote zone of the infarcted hearts were isolated using a previously published protocol (18). Briefly, left ventricle tissue was placed in a pre-chilled petri dish on ice and gently minced with small dissection scissors in mitochondrial isolation buffer (220mM mannitol, 70mM sucrose, 5mM MOPS, 1mM EGTA, pH 7.2 with KOH). Left ventricle fragments were transferred to 2mL of mitochondrial isolation buffer with 0.2% BSA and homogenized using a prechilled motor-driven teflon potter-elvehjem tissue homogenizer. The homogenate was centrifuged at 800g for 10min. The supernatant was collected and centrifuged at 9,000g for 15min. The resulting enriched mitochondrial pellet was resuspended in 1mL of mitochondrial isolation buffer and centrifuged at 10,000g for 10min. The resulting pellet of mitochondria was resuspended in 1mL mitochondrial isolation buffer and mitochondrial protein concentration was measured using a Pierce BCA Protein Assay kit according to manufacturer's protocol. Mitochondrial protein aliquots (50μg) were prepared and snap frozen in liquid nitrogen for downstream assays.

**Blue-Native polyacrylamide gel electrophoresis (BN PAGE)**

*Sample solubilization*

Enriched mitochondrial pellets were resuspended in solubilization buffer (50mM NaCl, 50mM imidazole/HCl, 2mM 6-aminohexanoic acid, 1mM EDTA, pH 7.0) with digitonin (8g digitonin/g mitochondrial protein) as previously described (25). After solubilization, samples were

centrifuged at 20,000g for 20 min at 4˚C. Glycerol and Coomassie G-250 were added to the resulting supernatant.

*Gradient gel preparation*

3-13% large gradient gels were hand-cast using the PROTEAN® II xi cell system (BioRad 1651801). Gradient gel composition was calculated according to previously published protocols (26). Briefly, 16x20cm and 20x20cm glass plate sandwiches were secured with clamps and set up in casting stands. A leveled gradient former (BioRad 165-4120) was placed on a magnetic stir plate and attached to thin plastic tubing inserted into each gel sandwich. Gels were cast by quickly pouring the 3% and 13% acrylamide solutions into the chambers and mixing at a constant stirring rate while pouring the gels.

*Gel electrophoresis*

Samples and molecular weight markers (NativeMark LC0725; ThermoFisher) were loaded to in-house cast 3-13% acrylamide gradient gels for electrophoresis using the PROTEAN® II xi cell system (BioRad 1651801). Gels were run at 150V for 1.5hr at 4˚C in dark cathode buffer (50 mM Tricine, 7.5mM Imidazole, 0.02% Coomassie blue G-250, pH 7.0), and switched to light cathode buffer (50 mM Tricine, 7.5mM Imidazole, 0.002% Coomassie blue G-250, pH 7.0) at 200V overnight at 4˚C.

*Coomassie staining*

After gel electrophoresis, gels were immediately transferred to a Coomassie fixing staining solution (50% (v/v) methanol, 10% (v/v) acetic acid, 0.025% (w/v) Coomassie dye) for 1hr. Gels

were destained in destaining solution (10% (v/v) acetic acid) for 4hrs. Gels were imaged on a backlit tray with a camera. Supercomplex bands were excised from the gel using a disposable grid cutter and mount (MEE2-9-34 and MEF67-9) to excise 11 bands 2mmx9mm in size in the supercomplex molecular weight region.

*In-gel digestion*

To ensure consistent profiling of the supercomplex bands across all samples, a gel cutter (MEE2-9-34 and MEF67-9 Gel Company) was used to excise 11 higher molecular weight supercomplex bands in each gel lane. Each gel band was cut into 5 smaller ($1mm^3$) pieces and destained with destaining solution (100mM ammonium bicarbonate, 30% acetonitrile) for 5 min by vortexing. This was repeated until all pieces were fully destained. Gel pieces were submerged in acetonitrile to dehydrate, and the gel pieces were left to dry. Trypsin (5ng/µL Promega V511C) in 50mM ammonium bicarbonate was added to each sample, and gel pieces were incubated overnight at 37˚C. The supernatant containing digested peptides was removed the following day and stored at -80˚C. Samples were then processed for liquid chromatography-tandem mass spectrometry.

**Liquid chromatography-tandem mass spectrometry**

Digested peptides were resuspended in 25mM ABC and 1% formic acid and transferred to a 96 well plate. The plate was loaded onto a nanoflow ultra-high-performance liquid chromatography (nanoLC) system (reversed-phase UltiMate™ 3000 RSLCnano System with ProFlow Meter (Thermo Fisher Scientific, Waltham, MA)) coupled with Orbitrap Eclipse™ Tribrid™ mass spectrometer (Thermo Fisher Scientific). Approximately 0.1 µg of the peptides was injected and separated on the nanoLC system, which involved cleanup on 3 µm PepMaps® C18 trap (Thermo

Fisher, 300 µm I.D. × 0.5 mm) followed by separation on a 72 min step-wise gradient from 6% to 85% solvent B (100% acetonitrile and 0.1% formic acid) on a 1.7 µm BEH130C18 nanoLC column (Waters, Milford, MA, USA, 100 µm I.D. × 10 cm). The eluted peptides were ionized by electrospray ionization in positive ion mode and full MS scans were acquired in the Orbitrap between 350 and 1800 m/z in profile mode at a 60,000 resolution. This was followed by Higher-energy Collisional Dissociation fragmentation and data-dependent acquisition (DDA) MS/MS analysis in the linear ion-trap of the instrument. All data were recorded with Xcalibur software (Thermo Fisher Scientific).

**Bioinformatic analyses**

*Mass spectrometry data analysis*

Raw mass spectrometry data were processed with MaxQuant version 2.6.7.0 using default settings if not stated otherwise. MS/MS spectra were analyzed using the andromeda search engine integrated into the MaxQuant environment. Searches were performed against the Uniprot-mouse reference proteome (UniProt proteome ID UP000000589) containing 45,742 protein entries. Oxidation (M), Acetyl (Protein N-terminal) were selected as variable modifications and carbamidomethyl (C) as a fixed modification. Label free quantification (LFQ) and 'match between runs' options were enabled. For peptide and protein identification, the false discovery rate (FDR) was set to 0.01. Minimal peptide length was set to 7 amino acids, and a maximum of 2 missed cleavages was allowed. The minimum number of razor peptides for protein identification was 1, and all proteins identified had at least 1 minimum unique peptide. Peptide and protein identifications were validated using a target-decoy approach in revert mode.

To remove any non-mitochondrial proteins, the resulting dataset was filtered to only include mitochondrial proteins according to the mouse MitoCarta 3.0 dataset (27). For the annotation of proteins using the MitoCarta functional annotations, proteins that had multiple annotations were included in each category in Fig 2E. Proteins that had no functional annotation in MitoCarta (OCIAD1 and GATD3) were manually assigned to a functional group. To account for batch-to-batch variability, LFQ intensities were normalized using a median normalization approach whereby raw LFQ intensities were normalized to the band median and total dataset median (28). Resulting LFQ intensities were filtered to only include proteins that had values for 2 of 4 samples in each group (sham and MI). LFQ intensities were $\log_2$ transformed prior to imputation and statistical analysis. Missing values were imputed using a global imputation strategy by imputing the group mean of the non-missing values in the sham and MI groups.

For complexome data analysis, Z-scores were calculated in Python using the Pandas and SciPy libraries (29, 30). Differentially expressed proteins were identified using limma (31) and visualized using the EnhancedVolcano package (32).

**Statistical analysis**

Unless stated or specified, all results for *in vivo* echocardiography and cardiac anatomy are shown as mean ± SEM. Graphpad Prism software 10.2.3 was used to calculate significance using an unpaired Student's t-test.

For complexome profiling analyses, Bayesian-modified t-tests with Benjamini-Hochberg correction were calculated using the limma package (31). Significance for differential expressed

proteins within each band was determined by a $\log_2$ fold-change cutoff of |0.58| and $-\log_{10}$ adjusted p-value cutoff of |1.3|.

## Results

### Myocardial infarction surgery induces cardiac dysfunction

To investigate the mitochondrial changes occurring in heart failure, male and female mice were subjected to MI surgery involving the permanent ligation of the left anterior descending artery (LAD). At 4 weeks post-MI, 2-dimensional echocardiography was employed to confirm cardiac dysfunction followed by mitochondrial isolations at 5 weeks post-MI (Fig 1A). Male mice that underwent MI surgery had increased heart weight to body weight ratios (HW/BW) (Fig 1B) and decreased ejection fraction (Fig 1C) along with increased end diastolic volume (EDV) (Fig 1D) and increased end systolic volume (ESV) compared to sham mice (Fig 1E). To quantify MI size, we measured akinetic length from the parasternal long axis view at 1 week and 4 weeks post-MI (Fig 1F) with male mice displaying an increased akinetic length at 4 weeks post-MI (Fig 1G). Female MI mice exhibited the same cardiac structural remodeling showing increased heart weight to body weight ratio (Fig S1A). Female MI mice also exhibited changes in cardiac function including decreased ejection fraction (Fig S1B), increased EDV (Fig S1C), increased ESV (Fig S1D), and increased akinetic length (Fig S1E-F) at 4wks post-MI.

### Complexome profiling identifies diverse mitochondrial proteins within the cardiac supercomplex proteome

To examine the proteome of supercomplexes in response to myocardial infarction, we employed an integrated Blue-Native PAGE and mass spectrometry approach, an emerging technique in mitochondrial research known as complexome profiling (Fig 2A). Mitochondria from the remote zone of the infarcted hearts were used for analysis as this region is adjacent to the site of direct infarct and maintains contractile function. To properly extract and solubilize supercomplexes from mitochondrial samples, the digitonin/mitochondrial protein ratio was optimized to resolve and maintain the higher molecular weight supercomplex assemblies before loading onto a Blue-Native PAGE gel (Fig S2A). After Coomassie staining, 11 gel bands from the supercomplex gel region were excised using a standard gel multi-band cutter and digested followed by LC-MS/MS to identify proteins within each band (Fig 2B). The majority of proteins identified were mitochondrial (approximately 83%) along with a small fraction of non-mitochondrial proteins (e.g., cytosol and endoplasmic reticulum), as expected, due to our use of a differential centrifugation mitochondrial isolation protocol. As our focus was to resolve mitochondrial protein complexes, the dataset was filtered using the Mouse MitoCarta3.0 database (27) to include only mitochondrial proteins present in at least 2 of 4 samples in the sham and MI groups. We identified between 168-187 mitochondrial proteins in each of the supercomplex bands (Fig 2C). Of these, approximately 96% of proteins were detected in two or more bands, and 70% of proteins were detected across all bands, indicative of a core set of co-migrating proteins including the electron transport chain proteins and other mitochondrial proteins. Confirming our excision of mitochondrial supercomplex bands, OXPHOS proteins made up over 85% of the protein abundance across all 11 bands as measured by the summed LFQ intensity of all OXPHOS proteins (Fig 2D). Using the Mouse MitoCarta3.0 biological pathway annotations

(27), we identified proteins involved in diverse functions across the supercomplex bands including OXPHOS, metabolism, mitochondrial central dogma, mitochondrial dynamics, protein import, sorting and homeostasis, small molecule transport, and signaling (Fig 2E). To assess the relative distribution of OXPHOS subunits across the bands, we compared the LFQ intensities of all OXPHOS proteins, identifying an enrichment of CI and CIII in band 2 and enriched CIV in band 1 and bands 5-9 in both sham and MI supercomplexes (Fig 3A). CV oligomeric chains co-migrated with the supercomplexes, as previously described in skeletal muscle (33).

**Myocardial infarction induces changes in the relative abundance of OXPHOS, metabolic, redox and ribosomal proteins within supercomplexes**

To investigate the composition of mitochondrial supercomplexes in heart failure, we assessed the relative abundance of proteins in excised bands from cardiac mitochondria of MI mice compared to sham mice. Several differences in protein abundance were identified across the 11 bands (Fig 4; Fig S3A). We first identified changes in OXPHOS proteins including increased abundance of mitochondrially encoded CI subunit, ND2 in bands 5 and 7, and CI subunit, NDUFS8 in band 7 (Fig S3A). Noted also were trends for lower abundance of CI subunits NDUFA3 and NDUFB10 in band 2. CIV subunits, COX6A1 and COX7A2 had increased abundance in band 5 and similarly COX6A2 increased in bands 3, 5, and 8 of MI supercomplexes compared to sham. Finally, CYCS, a crucial electron carrier protein, had increased abundance in MI supercomplex band 5 compared to sham.

In addition to changes in the relative abundance of OXPHOS proteins, multiple metabolic proteins displayed decreased abundance across MI supercomplexes. One subunit of the α-ketoglutarate dehydrogenase complex, DLST, had decreased abundance in MI bands 4 and 5 compared to sham supercomplex bands. In addition, trending decreases in OGDH and DLD, which are other subunits of the α-ketoglutarate dehydrogenase complex, were observed across the MI supercomplex bands. IDH2, a TCA cycle enzyme that catalyzes isocitrate to α-ketoglutarate conversion, producing NADPH, which is crucial for mitigating ROS accumulation and thus protecting against oxidative stress, had decreased abundance in MI band 10 compared to sham supercomplexes. Other metabolic proteins including PCCB, MCCC1, and MCCC2 decreased in various MI bands compared to sham bands across the dataset. Alongside these alterations in metabolic protein complexes, we identified a decrease in the relative abundance of SOD2, a redox signaling protein that converts the proximal form of mitochondrial ROS (i.e., superoxide) to hydrogen peroxide, across bands 2,3, and 10 in MI samples compared to sham samples. Finally, FAM162A, a protein involved in hypoxia-induced cell death, was increased in bands 2, 3, and 7 of the MI mitochondria compared to sham mitochondria.

Another class of mitochondrial protein complexes, the mitochondrial ribosomal proteins, were altered in MI supercomplexes compared to sham supercomplexes. The relative abundance of large ribosomal subunit proteins including MRPL50 was increased in band 8 and decreased in band 10 while MRPL12 was decreased in bands 9 and 10. Similarly, the relative abundances of the mitochondrial small ribosome subunit were changed across bands including an increase in MRPS16 and decrease in MRPS23, MRPS27, MRPS34, MRPS5, MRPS22, MRPS7 and MRPS35 across the MI supercomplex bands compared to the sham bands.

## Discussion

In the present study, we employed an emerging technique, complexome profiling, to identify over 180 mitochondrial proteins in supercomplex bands using Blue-Native PAGE combined with mass spectrometry. Using this technique to investigate mitochondria from ventricular tissue post-ischemic injury, we identified changes in the relative abundance of OXPHOS complexes, metabolic complexes, redox proteins, and ribosomal complexes within higher molecular weight supercomplex bands.

Heart failure is a complex disease characterized by mitochondrial dysfunction with evidence of altered supercomplex assembly. In human heart failure, previous work has shown no changes in CIV supercomplex in-gel activity compared to non-failing hearts but increased supercomplex activity after treatment with a mitochondrial-targeted tetrapeptide, Elamipretide, which can decrease the production of reactive oxygen species and stabilize cardiolipin (34, 35). In mitochondria from a pacing-induced canine model of heart failure, supercomplex assembly was decreased, as assessed by Blue-Native PAGE and immunoblotting (7). Our data further highlight how supercomplex remodeling may play a role in heart failure pathology and the response to mitochondrial-targeted therapeutic interventions. A recent study using quantitative cross-linking technology to assess protein complex changes in a murine pressure-overload induced model of heart failure, identified changes in the assembly of metabolic proteins such as ketone-oxidation enzymes as well as decreased interactions between CIV subunits (36). While these data provide evidence of changes associated with global ventricular remodeling in a pressure-overload induced heart failure model, supercomplex formation has also been

investigated in response to ischemia/reperfusion injury where the formation of an extra-large respirasome, $I_2$+$III_2$, is cardioprotective (12). Our findings showing changes in the abundance of mitochondrial OXPHOS complexes, metabolic, and redox proteins further highlight the dynamic nature of supercomplex assembly in an infarct-induced model of heart failure. Our data also align with recent work showing that supercomplex assembly is responsive to different metabolic substrates (18), as well as apoptotic stimuli (23), all signaling pathways that are involved in heart failure. Mitochondrial processes are most affected in the ischemic region of an infarcted heart compared to the remote or border zone of the heart (37), and the remote zone is enriched for cardiac contractile signatures compared to all other regions in human hearts post-myocardial infarction (38). We investigated mitochondria isolated from the remote zone tissue for all proteomic analyses (Fig 1A) because it is this region that maintains cardiac contraction after ischemic injury and is thus of key functional significance. In addition to the known remodeling in the infarct zone, our data support the conclusion that mitochondrial processes in the remote region are impacted and may contribute to the development of heart failure over time.

Complexome profiling is an emerging technique used to decipher protein complex composition, novel assembly factors and the active remodeling of these proteins in health and disease. Recent work in cardiac mitochondria has shown that mitochondrial protein complexes from diverse functional clusters assemble and can be predicted using advanced statistical correlation tools (23). Other work in the heart has further supported the involvement of metabolic, redox, and scaffold proteins within higher order mitochondrial protein complexes (18, 19). In our results, we identified a reduced abundance of proteins involved in the α-ketoglutarate dehydrogenase complex in MI supercomplexes. Beyond the production of succinyl CoA, one of the functions of

the α-ketoglutarate dehydrogenase complex is the shuttling of NADH, which is also produced, to NNT for NADPH synthesis to protect against oxidative stress (39), which is relevant to pathogenic mechanisms in heart failure. Indeed, α-ketoglutarate supplementation is protective in a murine pressure overload model (40, 41). As well, levels of succinyl-CoA are decreased in the murine myocardium post-infarct (42), and α-ketoglutarate dehydrogenase activity is decreased in heart tissue from patients with ischemic cardiomyopathy despite no changes in the total protein levels of this enzyme (43). Our data contribute novel insights into the reduced abundance of α-ketoglutarate dehydrogenase complex subunits within higher molecular weight complexes (i.e., beyond total levels of the protein) in a murine heart failure model. As this complex is a key metabolic node linking the replenishment of TCA cycle intermediates through anaplerosis and biosynthetic processes through cataplerosis, our results suggest potential functional consequences for TCA cycle metabolism.

In addition to changes in intermediary metabolism proteins, we identified a consistent decrease in the relative abundance of SOD2 across the MI supercomplexes compared to the sham supercomplexes. SOD2 is a mitochondrial antioxidant enzyme that catalyzes the conversion of superoxide to hydrogen peroxide, and is thus the first step in the control of ROS produced by mitochondria (44). Hydrogen peroxide can act as an important redox signal, but sustained high levels can cause oxidative damage to proteins, lipids and DNA. To prevent damage, it is subsequently metabolized to water and oxygen by catalases, peroxidases, and peroxiredoxins (45). Our study and others investigating cardiac supercomplexes have identified SOD2 with confidence amongst the supercomplex bands (18) or with high likelihood of comigration with CI and CIII subunits (23). As CI and CIII are major contributors to mitochondrial ROS emission

(44, 46), decreased abundance of SOD2 within MI supercomplexes may be indicative of impaired capacity to control ROS and thus may be mechanistically linked to the increased oxidative stress characteristic of heart failure (47). Another oxidative stress-related protein, FAM162A, which is involved in hypoxia and apoptotic signaling, was increased across multiple MI supercomplex bands compared to sham samples. Consistent with previous findings in ventricular tissue from patients with ischemic and dilated cardiomyopathy, where FAM162A is enriched in the peri-infarct region (48), our data further implicate its involvement in mitochondrial remodeling in heart failure.

Proteins within another functional category that were altered in the MI supercomplex bands compared to the sham bands were the mitochondrial ribosome proteins. Across almost all 11 bands, we identified both increases and decreases in subunits of the large and small ribosomal complexes. Disruption of the mitoribosome complex formation, specifically by partial knockout of MRPS5, has shown protective effects on cardiomyocyte proliferation (49). In contrast, complete loss of MRPS5 leads to cardiac dysfunction and impaired metabolism (50). Although we did not observe global decreases in mitochondrial-encoded proteins in the MI supercomplexes, which would indicate a deficit in mitochondrial translation, our data further implicate abnormal mitoribosome assembly as a potential contributor to heart failure pathology, such as through decreased capacity for OXPHOS protein synthesis.

While our study provides insights about supercomplexes in heart failure, there are limitations to be considered. First, only male mice were used for the proteomics analyses. Despite similar functional changes between male and female mice post-MI, there may be sex-specific

differences in mitochondrial supercomplexes which we did not address in our study but should now be prioritized for future study. Due to substantial mass-spectrometry data acquisition and analysis time associated with profiling each individual gel band across all experimental replicates, we chose to profile only the supercomplex region bands (around 1000kDa and higher) rather than the whole gel slice, which would correspond to upwards of 60 bands per gel lane (22, 25). This limited our ability to understand the rearrangement of complexes into monomer or other lower molecular weight species. In addition, we acknowledge the dynamic nature of supercomplex assemblies, formed through non-covalent interactions. As such the supercomplex profiles identified here may represent the most stable interactions and additional transient protein associations may have not been identified. Finally, we cannot conclude that the proteins identified in our dataset are forming protein-protein interactions, which requires follow up such as additional Blue-Native PAGE, co-immunoprecipitation, or cross-linking mass spectrometry. Future work using these techniques is required to explore the stoichiometric arrangements of supercomplexes, multimer to monomer ratios of proteins identified and confirm the functional implications of the incorporation of these proteins into supercomplexes. Rather our data stand as a proteomics resource and hypothesis-generating dataset to give insight into alterations in supercomplex formation in heart failure such as altered electron transport chain protein abundance in supercomplexes and changes in α-ketoglutarate dehydrogenase complex assembly.

In conclusion, our study demonstrates that mitochondrial complexes undergo distinct remodeling in murine heart failure marked by changes in the relative abundance of electron transport chain, metabolic, redox and ribosomal proteins, revealing novel changes in the mitochondrial proteome after myocardial infarction. Findings highlight the importance of investigating mitochondrial

supercomplex formation in cardiovascular disease to improve the understanding of metabolic and mitochondrial dysfunction.

## Data availability

All data are available from the corresponding authors upon reasonable request.

## Supplemental material

Supplemental Figures 1-3: https://doi.org/10.6084/m9.figshare.29213228


## Acknowledgments

We thank Megan Fortier of the uOttawa in vivo cardiac surgical core facility for completing all myocardial infarction surgeries. We thank Animal Care and Veterinary Services at the University of Ottawa. We thank Sam Williamson and Luc Tessier for mass spectrometry maintenance and running of system suitability tests and also thank Nicolas Lafrenière and Alexandra Star for help with mass spectrometry methods.

Schematic figures were created using Biorender.com (publication license: JR285IGGRI, NV285IGNMW).

Graphical Abstract: Created in BioRender. Fong-McMaster, C. (2025) https://BioRender.com/rx496ae

## Grants

463 This study was supported by a UOHI ORACLE Grant to M-E.H. and E.E.M., Heart and Stroke
464 Grant-in-Aid to M-E.H., Heart and Stroke New Investigator Award to E.E.M, and CIHR Grants
465 (E.E.M.-186076, M-E.H.-143278). C.F-M. and S.M.P. were supported by CIHR Canada
466 Graduate Scholarship Frederick Banting and Charles Best Doctoral Awards. S.M. and E.M. were
467 supported by OISB-NRC Graduate Student Scholarships.
468

469 **Disclosures**

470 No conflicts of interest, financial or otherwise, are declared by the authors.
471

472 **Author Information**

473 C.F-M., A.S.H., E.E.M, and M-E.H. conceived and designed research; C.F-M, S.M., S.M.P.,
474 G.G., I.L.S., and A.S.H. performed experiments; C.F-M., E.M., M.M.L., and A.S.H. analyzed
475 data; C.F-M., E.M., M.C.C., A.S.H., E.E.M., and M-E.H. interpreted results of experiments; C.F-
476 M., E.M. and M.M.L. prepared figures; C.F-M. drafted manuscript; S.M.P., M.C.C., A.S.H.,
477 E.E.M. and M-E.H. edited and revised manuscript, all authors approved final version of
478 manuscript.

## References


1. **Letts JA**, **Sazanov LA**. Clarifying the supercomplex: the higher-order organization of the mitochondrial electron transport chain. *Nat Struct Mol Biol* 24: 800–808, 2017. doi: 10.1038/nsmb.3460.

2. **Wittig I**, **Carrozzo R**, **Santorelli FM**, **Schägger H**. Supercomplexes and subcomplexes of mitochondrial oxidative phosphorylation. *Biochim Biophys Acta BBA - Bioenerg* 1757: 1066–1072, 2006. doi: 10.1016/j.bbabio.2006.05.006.

3. **Reifschneider NH**, **Goto S**, **Nakamoto H**, **Takahashi R**, **Sugawa M**, **Dencher NA**, **Krause F**. Defining the Mitochondrial Proteomes from Five Rat Organs in a Physiologically Significant Context Using 2D Blue-Native/SDS-PAGE. *J Proteome Res* 5: 1117–1132, 2006. doi: 10.1021/pr0504440.

4. **Gómez LA**, **Monette JS**, **Chavez JD**, **Maier CS**, **Hagen TM**. Supercomplexes of the mitochondrial electron transport chain decline in the aging rat heart. *Arch Biochem Biophys* 490: 30–35, 2009. doi: 10.1016/j.abb.2009.08.002.

5. **Hou T**, **Zhang R**, **Jian C**, **Ding W**, **Wang Y**, **Ling S**, **Ma Q**, **Hu X**, **Cheng H**, **Wang X**. NDUFAB1 confers cardio-protection by enhancing mitochondrial bioenergetics through coordination of respiratory complex and supercomplex assembly. *Cell Res* 29: 754–766, 2019. doi: 10.1038/s41422-019-0208-x.

6. **Chavez JD**, **Lee CF**, **Caudal A**, **Keller A**, **Tian R**, **Bruce JE**. Chemical Crosslinking Mass Spectrometry Analysis of Protein Conformations and Supercomplexes in Heart Tissue. *Cell Syst* 6: 136-141.e5, 2018. doi: 10.1016/j.cels.2017.10.017.

7. **Rosca MG**, **Vazquez EJ**, **Kerner J**, **Parland W**, **Chandler MP**, **Stanley W**, **Sabbah HN**, **Hoppel CL**. Cardiac mitochondria in heart failure: decrease in respirasomes and oxidative phosphorylation. *Cardiovasc Res* 80: 30–39, 2008. doi: 10.1093/cvr/cvn184.

8. **Kanaan GN**, **Patten DA**, **Redpath CJ**, **Harper M-E**. Atrial Fibrillation Is Associated With Impaired Atrial Mitochondrial Energetics and Supercomplex Formation in Adults With Type 2 Diabetes. *Can J Diabetes* 43: 67-75.e1, 2019. doi: 10.1016/j.jcjd.2018.05.007.

9. **Jang S**, **Lewis TS**, **Powers C**, **Khuchua Z**, **Baines CP**, **Wipf P**, **Javadov S**. Elucidating Mitochondrial Electron Transport Chain Supercomplexes in the Heart During Ischemia–Reperfusion. *Antioxid Redox Signal* 27: 57–69, 2017. doi: 10.1089/ars.2016.6635.

10. **Ramírez-Camacho I**, **Correa F**, **El Hafidi M**, **Silva-Palacios A**, **Ostolga-Chavarría M**, **Esparza-Perusquía M**, **Olvera-Sánchez S**, **Flores-Herrera O**, **Zazueta C**. Cardioprotective strategies preserve the stability of respiratory chain supercomplexes and reduce oxidative stress in reperfused ischemic hearts. *Free Radic Biol Med* 129: 407–417, 2018. doi: 10.1016/j.freeradbiomed.2018.09.047.

11. **Lotz C**, **Zhang J**, **Fang C**, **Liem D**, **Ping P**. Isoflurane Protects the Myocardium Against Ischemic Injury via the Preservation of Mitochondrial Respiration and Its Supramolecular Organization. *Anesth Analg* 120: 265–274, 2015. doi: 10.1213/ANE.0000000000000494.

12. **Liang C**, **Padavannil A**, **Zhang S**, **Beh S**, **Robinson DRL**, **Meisterknecht J**, **Cabrera-Orefice A**, **Koves TR**, **Watanabe C**, **Watanabe M**, **Illescas M**, **Lim R**, **Johnson JM**, **Ren S**, **Wu Y-J**, **Kappei D**, **Ghelli AM**, **Funai K**, **Osaka H**, **Muoio D**, **Ugalde C**, **Wittig I**, **Stroud DA**, **Letts JA**, **Ho L**. Formation of I2+III2 supercomplex rescues respiratory chain defects. *Cell Metab* 37: 441-459.e11, 2025. doi: 10.1016/j.cmet.2024.11.011.

13. **Wong R**, **Aponte AM**, **Steenbergen C**, **Murphy E**. Cardioprotection leads to novel changes in the mitochondrial proteome. *Am J Physiol-Heart Circ Physiol* 298: H75–H91, 2010. doi: 10.1152/ajpheart.00515.2009.

14. **Chapa-Dubocq XR**, **Rodríguez-Graciani KM**, **Guzmán-Hernández RA**, **Jang S**, **Brookes PS**, **Javadov S**. Cardiac Function is not Susceptible to Moderate Disassembly of Mitochondrial Respiratory Supercomplexes. *Int J Mol Sci* 21: 1555, 2020. doi: 10.3390/ijms21051555.

15. **Milenkovic D**, **Misic J**, **Hevler JF**, **Molinié T**, **Chung I**, **Atanassov I**, **Li X**, **Filograna R**, **Mesaros A**, **Mourier A**, **Heck AJR**, **Hirst J**, **Larsson N-G**. Preserved respiratory chain capacity and physiology in mice with profoundly reduced levels of mitochondrial respirasomes. *Cell Metab* 35: 1799-1813.e7, 2023. doi: 10.1016/j.cmet.2023.07.015.

16. **Cuillerier A**, **Burelle Y**. Hybrid Clear/Blue Native Electrophoresis for the Separation and Analysis of Mitochondrial Respiratory Chain Supercomplexes. *J Vis Exp* : 59294, 2019. doi: 10.3791/59294.

17. **Jha P**, **Wang X**, **Auwerx J**. Analysis of Mitochondrial Respiratory Chain Supercomplexes Using Blue Native Polyacrylamide Gel Electrophoresis (BN-PAGE). *Curr Protoc Mouse Biol* 6: 1–14, 2016. doi: 10.1002/9780470942390.mo150182.

18. **Zheng Y**, **Gibb AA**, **Xu H**, **Liu S**, **Hill BG**. The metabolic state of the heart regulates mitochondrial supercomplex abundance in mice. *Redox Biol* 63: 102740, 2023. doi: 10.1016/j.redox.2023.102740.

19. **Heide H**, **Bleier L**, **Steger M**, **Ackermann J**, **Dröse S**, **Schwamb B**, **Zörnig M**, **Reichert AS**, **Koch I**, **Wittig I**, **Brandt U**. Complexome Profiling Identifies TMEM126B as a Component of the Mitochondrial Complex I Assembly Complex. *Cell Metab* 16: 538–549, 2012. doi: 10.1016/j.cmet.2012.08.009.

20. **Gonzalez-Franquesa A**, **Stocks B**, **Chubanava S**, **Hattel HB**, **Moreno-Justicia R**, **Peijs L**, **Treebak JT**, **Zierath JR**, **Deshmukh AS**. Mass-spectrometry-based proteomics reveals mitochondrial supercomplexome plasticity. *Cell Rep* 35: 109180, 2021. doi: 10.1016/j.celrep.2021.109180.

21. **Van Strien J**, **Guerrero-Castillo S**, **Chatzispyrou IA**, **Houtkooper RH**, **Brandt U**, **Huynen MA**. COmplexome Profiling ALignment (COPAL) reveals remodeling of mitochondrial protein complexes in Barth syndrome. *Bioinformatics* 35: 3083–3091, 2019. doi: 10.1093/bioinformatics/btz025.

22. **Schulte U**, **Den Brave F**, **Haupt A**, **Gupta A**, **Song J**, **Müller CS**, **Engelke J**, **Mishra S**, **Mårtensson C**, **Ellenrieder L**, **Priesnitz C**, **Straub SP**, **Doan KN**, **Kulawiak B**, **Bildl W**, **Rampelt H**, **Wiedemann N**, **Pfanner N**, **Fakler B**, **Becker T**. Mitochondrial complexome reveals quality-control pathways of protein import. *Nature* 614: 153–159, 2023. doi: 10.1038/s41586-022-05641-w.

23. **Rigoni G**, **Calvo E**, **Glytsou C**, **Carro-Alvarellos M**, **Noguchi M**, **Semenzato M**, **Quirin C**, **Caicci F**, **Meneghetti N**, **Sturlese M**, **Ishihara T**, **Moro S**, **Rampazzo C**, **Ishihara N**, **Bezzo F**, **Salviati L**, **Vazquez J**, **Sales G**, **Romualdi C**, **Enriquez JA**, **Scorrano L**, **Soriano ME**. MARIGOLD and MitoCIAO, two searchable compendia to visualize and functionalize protein complexes during mitochondrial remodeling. .

24. **Dann MM**, **Clark SQ**, **Trzaskalski NA**, **Earl CC**, **Schepers LE**, **Pulente SM**, **Lennord EN**, **Annamalai K**, **Gruber JM**, **Cox AD**, **Lorenzen-Schmidt I**, **Seymour R**, **Kim K-H**, **Goergen CJ**, **Mulvihill EE**. Quantification of murine myocardial infarct size using 2-D and 4-D high-frequency ultrasound. *Am J Physiol Heart Circ Physiol* 322: H359–H372, 2022. doi: 10.1152/ajpheart.00476.2021.

25. **Giese H**, **Meisterknecht J**, **Heidler J**, **Wittig I**. Mitochondrial Complexome Profiling. *Methods Mol Biol Clifton NJ* 2192: 269–285, 2021. doi: 10.1007/978-1-0716-0834-0_19.

26. **Wittig I**, **Braun H-P**, **Schägger H**. Blue native PAGE. *Nat Protoc* 1: 418–428, 2006. doi: 10.1038/nprot.2006.62.

27. **Rath S**, **Sharma R**, **Gupta R**, **Ast T**, **Chan C**, **Durham TJ**, **Goodman RP**, **Grabarek Z**, **Haas ME**, **Hung WHW**, **Joshi PR**, **Jourdain AA**, **Kim SH**, **Kotrys AV**, **Lam SS**, **McCoy JG**, **Meisel JD**, **Miranda M**, **Panda A**, **Patgiri A**, **Rogers R**, **Sadre S**, **Shah H**, **Skinner OS**, **To T-L**, **Walker MA**, **Wang H**, **Ward PS**, **Wengrod J**, **Yuan C-C**, **Calvo SE**, **Mootha VK**. MitoCarta3.0: an updated mitochondrial proteome now with sub-organelle localization and pathway annotations. *Nucleic Acids Res* 49: D1541–D1547, 2021. doi: 10.1093/nar/gkaa1011.

28. **Haqqani AS**, **Kelly JF**, **Stanimirovic DB**. Quantitative protein profiling by mass spectrometry using label-free proteomics. *Methods Mol Biol Clifton NJ* 439: 241–256, 2008. doi: 10.1007/978-1-59745-188-8_17.

29. **McKinney W**. Data Structures for Statistical Computing in Python. Python in Science Conference, p. 56–61.

30. **Virtanen P**, **Gommers R**, **Oliphant TE**, **Haberland M**, **Reddy T**, **Cournapeau D**, **Burovski E**, **Peterson P**, **Weckesser W**, **Bright J**, **van der Walt SJ**, **Brett M**, **Wilson J**, **Millman KJ**, **Mayorov N**, **Nelson ARJ**, **Jones E**, **Kern R**, **Larson E**, **Carey CJ**, **Polat İ**, **Feng Y**, **Moore EW**, **VanderPlas J**, **Laxalde D**, **Perktold J**, **Cimrman R**, **Henriksen I**, **Quintero EA**, **Harris CR**, **Archibald AM**, **Ribeiro AH**, **Pedregosa F**, **van Mulbregt P**. SciPy 1.0: fundamental algorithms for scientific computing in Python. *Nat Methods* 17: 261–272, 2020. doi: 10.1038/s41592-019-0686-2.

31. **Ritchie ME**, **Phipson B**, **Wu D**, **Hu Y**, **Law CW**, **Shi W**, **Smyth GK**. limma powers differential expression analyses for RNA-sequencing and microarray studies. *Nucleic Acids Res* 43: e47–e47, 2015. doi: 10.1093/nar/gkv007.

32. **Blighe K**, **Rana S**, **Lewis M**. EnhancedVolcano: Publication-ready volcano plots with enhanced colouring and labeling. *R Package Version* 1: 10–18129, 2018.

33. **Greggio C**, **Jha P**, **Kulkarni SS**, **Lagarrigue S**, **Broskey NT**, **Boutant M**, **Wang X**, **Conde Alonso S**, **Ofori E**, **Auwerx J**, **Cantó C**, **Amati F**. Enhanced Respiratory Chain Supercomplex Formation in Response to Exercise in Human Skeletal Muscle. *Cell Metab* 25: 301–311, 2017. doi: 10.1016/j.cmet.2016.11.004.

34. **Chatfield KC**, **Sparagna GC**, **Chau S**, **Phillips EK**, **Ambardekar AV**, **Aftab M**, **Mitchell MB**, **Sucharov CC**, **Miyamoto SD**, **Stauffer BL**. Elamipretide Improves Mitochondrial Function in the Failing Human Heart. *JACC Basic Transl Sci* 4: 147–157, 2019. doi: 10.1016/j.jacbts.2018.12.005.

35. **Kloner RA**, **Shi J**, **Dai W**. New therapies for reducing post-myocardial left ventricular remodeling. *Ann Transl Med* 3: 20, 2015. doi: 10.3978/j.issn.2305-5839.2015.01.13.

36. **Caudal A**, **Tang X**, **Chavez JD**, **Keller A**, **Mohr JP**, **Bakhtina AA**, **Villet O**, **Chen H**, **Zhou B**, **Walker MA**, **Tian R**, **Bruce JE**. Mitochondrial interactome quantitation reveals structural changes in metabolic machinery in the failing murine heart. *Nat Cardiovasc Res* 1: 855–866, 2022. doi: 10.1038/s44161-022-00127-4.

37. **Pulido M**, **de Pedro MÁ**, **Álvarez V**, **Marchena AM**, **Blanco-Blázquez V**, **Báez-Díaz C**, **Crisóstomo V**, **Casado JG**, **Sánchez-Margallo FM**, **López E**. Transcriptome Profile Reveals Differences between Remote and Ischemic Myocardium after Acute Myocardial Infarction in a Swine Model. *Biology* 12: 340, 2023. doi: 10.3390/biology12030340.

38. **Kuppe C**, **Ramirez Flores RO**, **Li Z**, **Hayat S**, **Levinson RT**, **Liao X**, **Hannani MT**, **Tanevski J**, **Wünnemann F**, **Nagai JS**, **Halder M**, **Schumacher D**, **Menzel S**, **Schäfer G**, **Hoeft K**, **Cheng M**, **Ziegler S**, **Zhang X**, **Peisker F**, **Kaesler N**, **Saritas T**, **Xu Y**, **Kassner A**, **Gummert J**, **Morshuis M**, **Amrute J**, **Veltrop RJA**, **Boor P**, **Klingel K**, **Van Laake LW**, **Vink A**, **Hoogenboezem RM**, **Bindels EMJ**, **Schurgers L**, **Sattler S**, **Schapiro D**, **Schneider RK**, **Lavine K**, **Milting H**, **Costa IG**, **Saez-Rodriguez J**, **Kramann R**. Spatial multi-omic map of human myocardial infarction. *Nature* 608: 766–777, 2022. doi: 10.1038/s41586-022-05060-x.

39. **Wagner M**, **Bertero E**, **Nickel A**, **Kohlhaas M**, **Gibson GE**, **Heggermont W**, **Heymans S**, **Maack C**. Selective NADH communication from α-ketoglutarate dehydrogenase to mitochondrial transhydrogenase prevents reactive oxygen species formation under reducing conditions in the heart. *Basic Res Cardiol* 115: 53, 2020. doi: 10.1007/s00395-020-0815-1.

40. **An D**, **Zeng Q**, **Zhang P**, **Ma Z**, **Zhang H**, **Liu Z**, **Li J**, **Ren H**, **Xu D**. Alpha-ketoglutarate ameliorates pressure overload-induced chronic cardiac dysfunction in mice. *Redox Biol* 46: 102088, 2021. doi: 10.1016/j.redox.2021.102088.

41. **Yu H**, **Gan D**, **Luo Z**, **Yang Q**, **An D**, **Zhang H**, **Hu Y**, **Ma Z**, **Zeng Q**, **Xu D**, **Ren H**. α-Ketoglutarate improves cardiac insufficiency through NAD+-SIRT1 signaling-mediated mitophagy and ferroptosis in pressure overload-induced mice. *Mol Med* 30: 15, 2024. doi: 10.1186/s10020-024-00783-1.

42. **Takada S**, **Maekawa S**, **Furihata T**, **Kakutani N**, **Setoyama D**, **Ueda K**, **Nambu H**, **Hagiwara H**, **Handa H**, **Fumoto Y**, **Hata S**, **Masunaga T**, **Fukushima A**, **Yokota T**, **Kang D**, **Kinugawa S**, **Sabe H**. Succinyl-CoA-based energy metabolism dysfunction in chronic heart failure. *Proc Natl Acad Sci* 119: e2203628119, 2022. doi: 10.1073/pnas.2203628119.

43. **Ali HR**, **Michel CR**, **Lin YH**, **McKinsey TA**, **Jeong MY**, **Ambardekar AV**, **Cleveland JC**, **Reisdorph R**, **Reisdorph N**, **Woulfe KC**, **Fritz KS**. Defining decreased protein succinylation of failing human cardiac myofibrils in ischemic cardiomyopathy. *J Mol Cell Cardiol* 138: 304–317, 2020. doi: 10.1016/j.yjmcc.2019.11.159.

44. **Murphy MP**. How mitochondria produce reactive oxygen species. *Biochem J* 417: 1–13, 2009. doi: 10.1042/BJ20081386.

45. **Sies H**. Hydrogen peroxide as a central redox signaling molecule in physiological oxidative stress: Oxidative eustress. *Redox Biol* 11: 613–619, 2017. doi: 10.1016/j.redox.2016.12.035.

46. **St-Pierre J**, **Buckingham JA**, **Roebuck SJ**, **Brand MD**. Topology of Superoxide Production from Different Sites in the Mitochondrial Electron Transport Chain. *J Biol Chem* 277: 44784–44790, 2002. doi: 10.1074/jbc.M207217200.

47. **Tsutsui H**, **Kinugawa S**, **Matsushima S**. Oxidative stress and heart failure. *Am J Physiol-Heart Circ Physiol* 301: H2181–H2190, 2011. doi: 10.1152/ajpheart.00554.2011.

48. **Lee S-H**, **Hadipour-Lakmehsari S**, **Kim DH**, **Di Paola M**, **Kuzmanov U**, **Shah S**, **Lee JJ-H**, **Kislinger T**, **Sharma P**, **Oudit GY**, **Gramolini AO**. Bioinformatic analysis of membrane and associated proteins in murine cardiomyocytes and human myocardium. *Sci Data* 7: 425, 2020. doi: 10.1038/s41597-020-00762-1.

49. **Gao F**, **Liang T**, **Lu YW**, **Pu L**, **Fu X**, **Dong X**, **Hong T**, **Zhang F**, **Liu N**, **Zhou Y**, **Wang H**, **Liang P**, **Guo Y**, **Yu H**, **Zhu W**, **Hu X**, **Chen H**, **Zhou B**, **Pu WT**, **Mably JD**, **Wang J**, **Wang D-Z**, **Chen J**. Reduced Mitochondrial Protein Translation Promotes Cardiomyocyte Proliferation and Heart Regeneration. *Circulation* 148: 1887–1906, 2023. doi: 10.1161/CIRCULATIONAHA.122.061192.

50. **Gao F**, **Liang T**, **Lu YW**, **Fu X**, **Dong X**, **Pu L**, **Hong T**, **Zhou Y**, **Zhang Y**, **Liu N**, **Zhang F**, **Liu J**, **Malizia AP**, **Yu H**, **Zhu W**, **Cowan DB**, **Chen H**, **Hu X**, **Mably JD**, **Wang J**, **Wang D-Z**, **Chen J**. A defect in mitochondrial protein translation influences mitonuclear communication in the heart. *Nat Commun* 14: 1595, 2023. doi: 10.1038/s41467-023-37291-5.

## Figure Legends

**Figure 1. Cardiac structure and function are altered at 4 weeks post-myocardial infarction.** **(A)** *In vivo* study design overview. (Created in BioRender. Fong-McMaster, C. (2025) https://BioRender.com/44wh05f.) **(B)** Heart weight/body weight (mg/g) was measured at 4 weeks post-myocardial infarction (MI) in male mice. **(C-E)** Cardiac functional parameters including ejection fraction (C), end-diastolic volume (D), and end-systolic volume (E) were measured at 4 weeks post-MI in male mice. **(F)** Representative parasternal long axis image at 1 week and 4 weeks post-myocardial infarction (MI) with total left ventricle distance in blue and akinetic distance in green. **(G)** Akinetic length was calculated as the akinetic distance/total distance x 100%. P-value calculated by a Student's t-test or paired t-test for 1 week and 4 week comparison. n=5-10 male mice per group (MI and sham).

**Figure 2. Identification of mitochondrial proteins within high molecular weight complexes using complexome profiling. (A)** Experimental approach to study MI and sham supercomplexes using Blue-Native PAGE, mass spectrometry and bioinformatic analyses. (Created in BioRender. Fong-McMaster, C. (2025) https://BioRender.com/k456uvx) **(B)** Representative Blue-Native PAGE gel with 11 excised bands from sham (n=4) and MI (n=4) male mice. **(C)** Number of mitochondrial proteins identified in sham and MI samples (minimum n=2) per band after filtering out non-mitochondrial proteins using the Mouse MitoCarta 3.0 database. **(D)** Abundance of oxidative phosphorylation (OXPHOS) proteins measured by the summed LFQ intensity of OXPHOS proteins compared to the summed LFQ intensity of all other proteins in sham supercomplex bands. **(E)** Functional annotation of proteins identified with the 11 supercomplex bands in sham and MI samples (minimum n=2) determined by MitoCarta 3.0 annotation. Proteins with multiple functional annotations were included in all relevant annotation groups.

**Figure 3. Distribution of OXPHOS complexes across supercomplex bands. (A)** Z-scored plot of all CI-CV complexes identified across 11 bands for sham and MI groups. Raw LFQ intensities were z-scored across bands. The maximum scale was set to 3 and minimum scale to -3.

**Figure 4. Myocardial infarction-induced changes in supercomplex proteins. (A)** Heatmap plot of $\log_2$fold-change of proteins with significant differential relative abundance between MI and sham supercomplex bands. Differential relative abundance was identified in at least 1 supercomplex band with significance cutoffs of $\log_2$ fold-change |0.58| and $-\log_{10}$ adjusted p-value |1.3|. n=4 male mice per group (MI and sham).

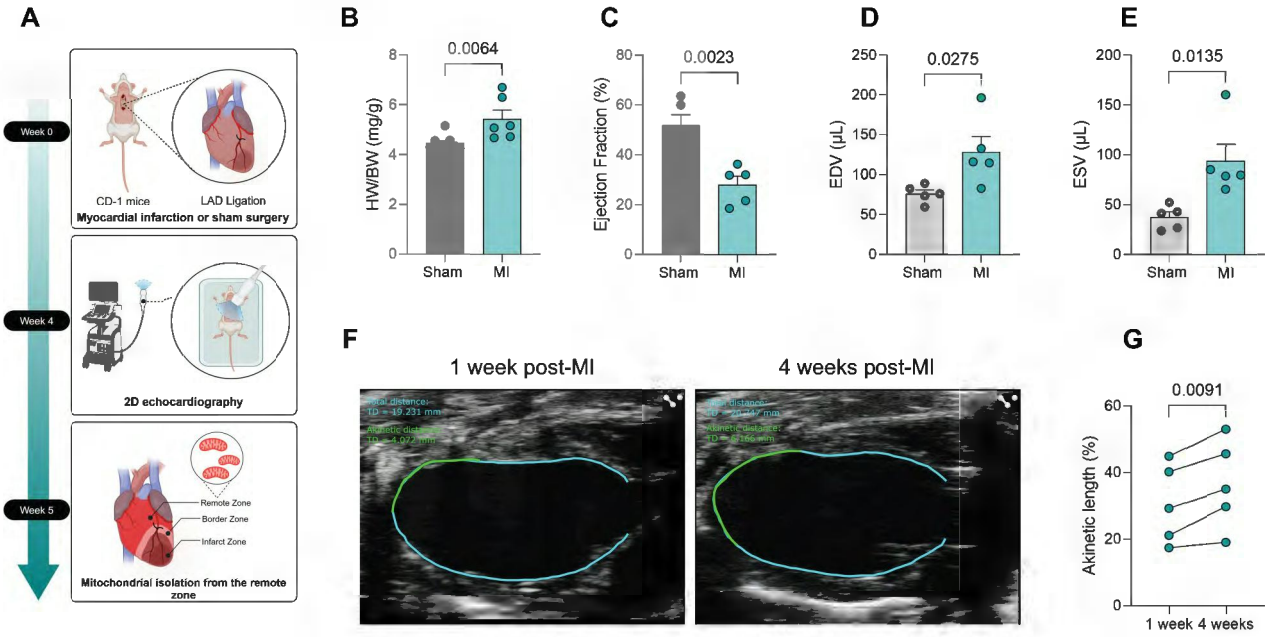
A
Week 0
CD-1 mice
LAD Ligation
Myocardial infarction or sham surgery
Week 4
2D echocardiography
Week 5
Remote Zone
Border Zone
Infarct Zone
Mitochondrial isolation from the remote zone
B
0.0064
HW/BW (mg/g)
Sham
MI
C
0.0023
Ejection Fraction (%)
Sham
MI
D
0.0275
EDV (μL)
Sham
MI
E
0.0135
ESV (μL)
Sham
MI
F
1 week post-MI
4 weeks post-MI
G
0.0091
Akinetic length (%)
1 week 4 weeks

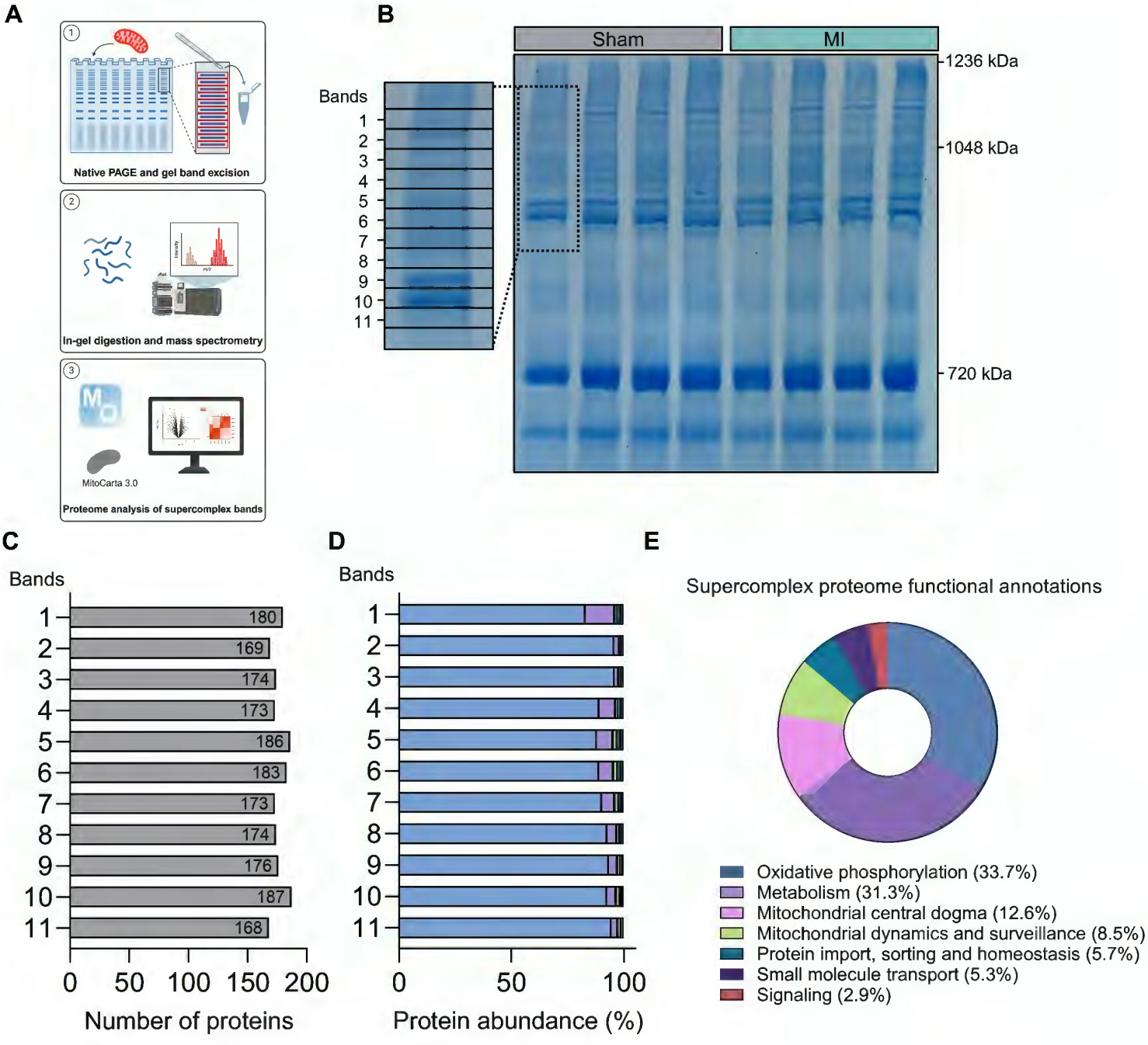
A
Native PAGE and gel band excision
In-gel digestion and mass spectrometry
MitoCarta 3.0
Proteome analysis of supercomplex bands
B
Sham
MI
Bands
1
2
3
4
5
6
7
8
9
10
11
1236 kDa
1048 kDa
720 kDa
C
Bands
180
169
174
173
186
183
173
174
176
187
168
0
50
100
150
200
Number of proteins
D
Bands
0
50
100
Protein abundance (%)
E
Supercomplex proteome functional annotations
Oxidative phosphorylation (33.7%)
Metabolism (31.3%)
Mitochondrial central dogma (12.6%)
Mitochondrial dynamics and surveillance (8.5%)
Protein import, sorting and homeostasis (5.7%)
Small molecule transport (5.3%)
Signaling (2.9%)

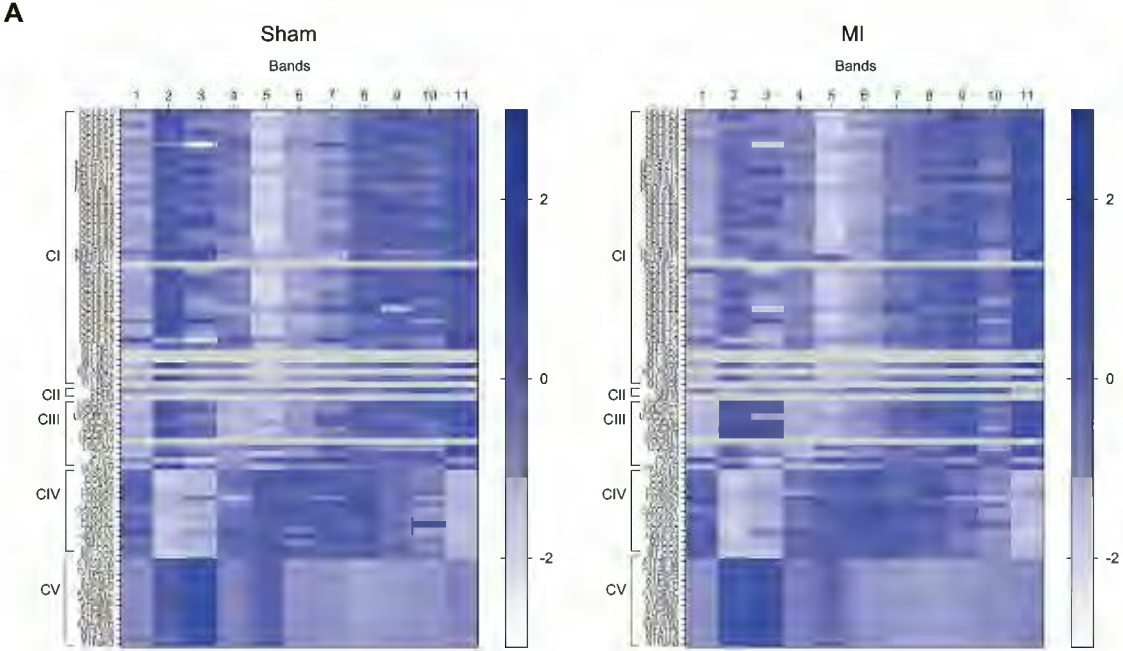
A
Sham
MI
Bands
1
2
3
4
5
6
7
8
9
10
11
CI
CII
CIII
CIV
CV
2
0
-2

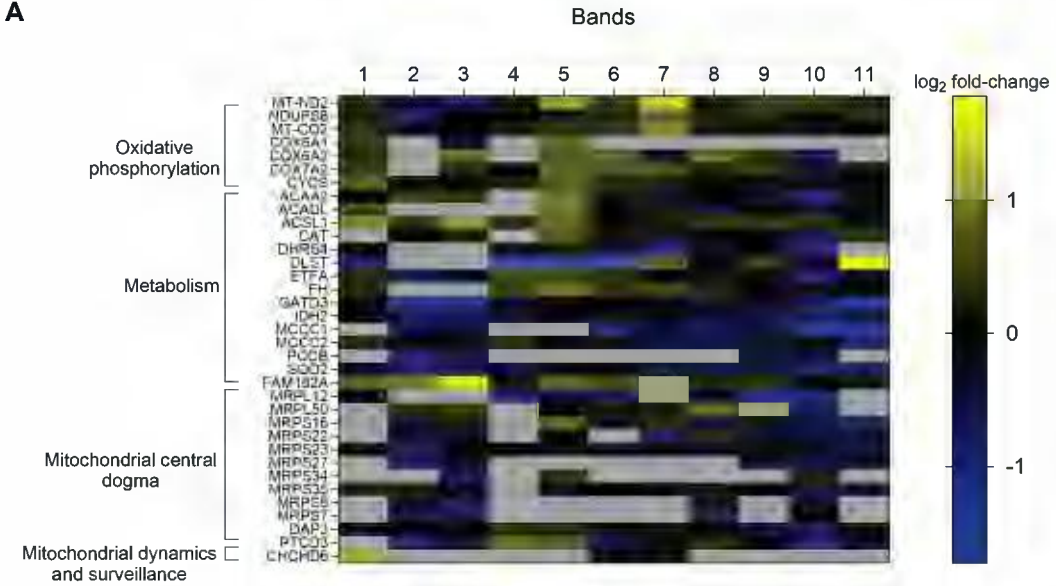
A
Bands
1
2
3
4
5
6
7
8
9
10
11
log2 fold-change
1
0
-1
Oxidative phosphorylation
Metabolism
Mitochondrial central dogma
Mitochondrial dynamics and surveillance
MT-ND2
NDUFS8
MT-CO2
COX6A1
COX6A2
COA7A2
CYCS
ACAA2
ACADL
ACSL1
CAT
DHRS4
DLST
ETFA
FH
GATD3
IDH2
MCCC1
MCCC2
POLB
SOD2
FAM182A
MRPL12
MRPL50
MRPS16
MRPS22
MRPS23
MRPS27
MRPS34
MRPS35
MRPS6
MRPS7
DAP3
PTCD3
CHCHD6

# Changes in mitochondrial supercomplexes in murine heart failure